Accessible Ratio-Specific Mixing: Single-Pressure-Driven Multi-Reagent Mixer Design and Synthesis for 3D-Printed Microfluidics

Yushen Zhang^{1*}, Debraj Kundu^{1*}, Tsun-Ming Tseng¹, Sudip Roy², Shigeru Yamashita³, Ulf Schlichtmann¹

¹Technical University of Munich, ²Indian Institute of Technology Roorkee, ³Ritsumeikan University

¹{yushen.zhang, debraj.kundu, tsun-ming.tseng, ulf.schlichtmann}@tum.de, ²sudip.roy@cs.iitr.ac.in,

³ger@fc.ritsumei.ac.jp

*These authors contributed equally.

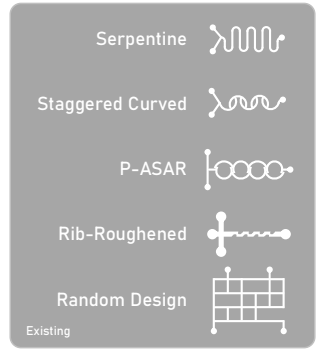
Abstract-Precise reagent mixing in user-defined ratios is a fundamental requirement in many microfluidic applications, including diagnostics, chemical synthesis, and biological assays. However, existing solutions for ratio-specific mixing often rely on complex active components, such as multiple pressure sources, flow controllers, or on-chip valves, making them costly, bulky, and unsuitable for portable or low-resource settings. In this work, we present a mixer design and a synthesis method for generating 3D-printable microfluidic devices that achieve ratiospecific mixing using only a single constant pressure source. Our method decomposes the desired mixing ratio into additive subcomponents, each represented by a dedicated inlet channel with a tailored length to enforce the correct hydraulic resistance. The method outputs a complete microfluidic layout, ready for direct fabrication via 3D printers. We validate our approach through numerical simulations and physical prototyping across eight diverse mixing scenarios. Results show that the achieved mixing ratios closely resemble the target, demonstrating the method's accuracy and robustness. This work enables low-cost, portable, and accessible microfluidic devices for ratio-specific solution delivery, broadening the scope of microfluidics in settings where simplicity, reproducibility, and affordability are critical.

I. INTRODUCTION

Microfluidics has emerged as a transformative technology across various scientific and industrial domains, enabling precise control and manipulation of fluids at the microscale. Precise reagent mixing in microfluidic systems is a critical requirement across various applications in diagnostics [1], chemical synthesis [2], and biological assays [3]. In these contexts, the ability to accurately combine multiple reagents in arbitrary, user-defined ratios is often essential for ensuring experimental validity and reproducibility. Traditionally, achieving such ratio-specific mixing has required either complex external instrumentation, such as multiple pressure sources, flow sensors, or on-chip valves. These systems, while effective, tend to increase cost, size, and operational complexity, which can hinder deployment in portable or point-of-care settings. Furthermore, scaling up such solutions for high-throughput or parallelized operations becomes cumbersome due to the increasing demand on external control hardware. Moreover, most conventional microfluidic chips are fabricated using

cleanroom-dependent processes like soft lithography. These methods are not only labor-intensive and expensive but also present a high barrier to entry for rapid prototyping or broad deployment outside well-equipped labs. In contrast, the rise of low-cost, high-resolution 3D printing technologies offers a promising alternative: fully digital, maskless fabrication of microfluidic devices with customized internal geometries [4].

Despite this opportunity, existing design approaches for passive microfluidic mixing are either limited to fixed, predetermined ratios or require manual trial-and-error to adjust channel lengths and resistances to match a desired output ratio. This process can be time-consuming and error-prone, particularly as the number of reagents or the complexity of the target ratio increases. Moreover, most available passive designs, like those depicted in Fig. 1, mostly focus on the homogeneity of the mixture and have only symmetric (e.g., 1:1) mixing ratios, inherently constraining the flexibility of the achievable ratios [5], [6]. Some recent efforts have explored randomized channel layouts to enhance mixing through chaotic advection. Wang et al. and Agrawal et al. explore the use of randomized spatial layouts to enhance mixing efficiency in passive systems



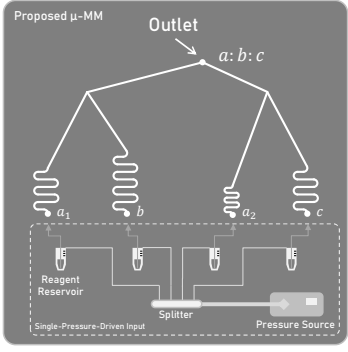


Fig. 1. Comparison of existing passive micromixer designs (left) and our proposed ratio-specific mixing layout (right). While traditional designs focus on homogeneity of the mixture, our method synthesizes a microfluidic network tailored for ratio-specific mixing for multiple reagents by decomposing each reagent's contribution (e.g., $a = a_1 + a_2$) into smaller subflows.

[7]–[9], but these approaches focus on homogenizing mixtures of sample and buffer only rather than achieving precise ratio control, particularly when multiple reagents must be combined in exact proportions.

In this work, we introduce μ -MM—a tree-shaped mixer design and a deterministic, algorithmic design synthesis method for generating 3D-printable microfluidic chips that produce multi-reagent target ratio mixing using only a single constant pressure source. Utilizing just a single pressure source along with 3D-printed chips makes this method highly appealing for portable, disposable, or low-cost diagnostic platforms, as well as for applications where power and equipment limitations prevent the use of active components. Our key idea is to decompose the given volumetric contribution of each reagent into smaller additive units. We will treat these units as inlet flow rates, which will serve as the basis for designing a microfluidic chip employing the electronic-hydraulic analogy. For example, a target ratio of 32:10:5 might be restructured as 16:8:8:4:6:5. These subcomponents are then treated as individual inlet flows, each routed through a channel with a precisely computed length to enforce the correct hydraulic resistance. Under a single shared pressure source, the system naturally balances flow rates such that the final mixture matches the desired ratios. To further enhance mixing performance without requiring active components, our algorithm strategically shuffles and reorders the subcomponents spatially across the device. This promotes greater interleaving of reagent flows, increasing the "spectrum width" of the laminar flow and improving homogeneity at the output. Our synthesis generates a complete chip design including inlet assignments, channel geometries, and exact 3D dimensions. The resulting file can be directly exported for additive manufacturing using 3D printers, removing the need for cleanroom facilities or manual tuning. We validate our approach by synthesizing and testing eight different chip designs, targeting both real-world and synthetic mixing ratio requirements. Simulation results show that the final output closely matches the intended mixing ratios, with minimal deviation. We also fabricate prototypes using hobby-grade 3D printers, demonstrating the manufacturability of our proposed synthesis results.

In summary, our work addresses a key gap in microfluidic design by enabling automatic generation of single-pressure, ratio-specific microfluidic mixers that are readily manufacturable via 3D printing. By shifting complexity from external hardware into algorithmic design, we lower barriers to adoption while expanding the practical capabilities of 3D-printed microfluidics for real-world applications. Our contributions are multi-fold:

- First, we propose a tree-shaped mixer design that enables multi-reagent mixing in specific ratios using a single pressure source, thereby reducing the need for complex external equipment and enabling low-cost microfluidics.
- Second, we propose a novel algorithm that decomposes the ratio proportions into smaller values based on a division approach to increase the homogeneity of the mixed solution.

- Third, we propose a method that considers each decomposed ratio-proportion as a flow rate for each inlet and defines the corresponding mix-flow tree.
- Fourth, we introduce a placement and routing method that synthesizes the chip layout based on an electrical circuit analogy and outputs 3D-printable design files.

The remainder of this paper is as follows: Section II introduces the background and related works; Section III details the proposed single-pressure-driven ratio-specific mixer design synthesis; Section IV presents the experimental results, with the conclusion provided in Section V.

II. MICROFLUIDIC MIXING

Mixing accuracy during multi-reagent mixing directly impacts result reliability and resolution, particularly when reagent concentrations or reaction kinetics are critical for specific biochemical applications. In biochemical assays and diagnostics, controlled mixing of enzymes, buffers, and samples is essential for detecting biomarkers via enzyme reactions, immunoassays, or nucleic acid amplification (e.g., PCR) [10]. Creating precise concentration gradients of candidate drugs in microchannels, vital for dose-response studies, relies on accurate mixing of stock solutions [11]. A particular challenge in mixing arises when the task is not simply to mix two fluids uniformly, but to mix multiple reagents in precise, user-defined ratios. This requirement is common in gradient generation [12], parallel assays [10], and combinatorial synthesis [13]. Achieving such targeted mixing ratios in a robust and programmable manner adds another layer of complexity to the design process, as it requires both accurate fluid handling and control over the spatiotemporal distribution of the flow.

Microfluidic mixers are broadly categorized into passive and active designs. Passive mixers, favored for their simplicity, ease of integration, and lack of external power, rely on channel geometry and flow (e.g., serpentine channels, staggered herringbone mixers, T-/Y-junctions) to stretch and fold fluid interfaces, accelerating diffusion [6], [14]. Active mixers, conversely, use external forces like acoustic waves [15], electric fields [16], or magnetic stirrers [17] to dynamically perturb flow and promote mixing, though this adds complexity and integration challenges. Designing mixers for specific, multiinput mixing ratios is less explored and often done ad hoc or manually. To address this, several computational and algorithmic design synthesis methods have been proposed. Tree-like dilution networks are a common approach [18], that generate a sequence of mixing steps to approximate desired concentrations. Some leverage analytical models of flow and mixing, optimizing channel geometries or flow splits to approximate desired outputs [14]. Others use graph-based methods [18]-[20], and aim to reduce reagent usage and minimize mixing steps. However, to generate the actual target ratios from those mixing sequences, we need additional scheduling, placement and routing operations for respective fluids. More recent work applies artificial intelligence or machine learning to automate design exploration [21], [22]. However, these methods merely

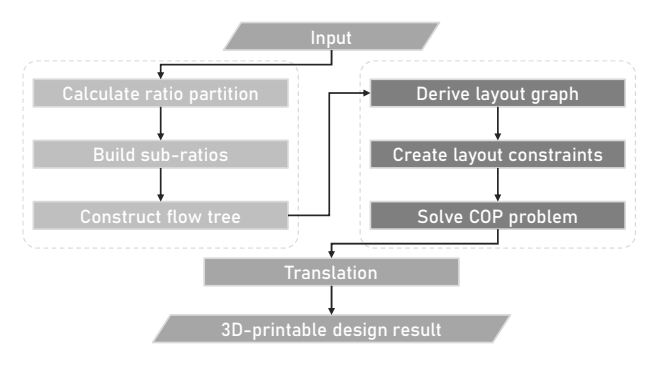


Fig. 2. Overview of proposed synthesis method.

focus on homogeneity and scalability, and less on the accuracy of multi-reagent ratio control.

Despite these advances, there remains a need for a systematic and scalable synthesis method that can automatically generate microfluidic mixer designs capable of producing precise and arbitrary mixing ratios across multiple inputs, while being compatible with affordable 3D printing microfluidic fabrication.

III. DESIGN SYNTHESIS METHOD

To enable passive, ratio-specific mixing of multiple reagents using a single pressure source, we propose a two-stage design synthesis method, as depicted in Fig. 2. Given a target ratio, in the first stage, our approach deterministically partitions and decomposes the ratios into sub-ratios and constructs a tree-shaped flow graph that ensures exact volumetric contributions. In the second stage, based on the electronic-hydraulic analogy, we determine the exact lengths of the channels corresponding to edges of the flow graph and generate an optimized layout placement of the channels utilizing constraint optimization programming to minimize the layout area.

A. Ratio Decomposition and Mix-Flow Tree Generation

Passive micro-mixers offer the advantage of eliminating external actuation systems, relying instead on channel geometry and internal fluid dynamics to achieve mixing. However, this simplification in actuation often comes at the cost of complex internal geometries designed to promote diffusion and mixing. To reduce this geometric complexity while still ensuring homogeneous mixing, we propose a deterministic synthesis method that generates a tree-shaped passive mixer optimized for a given target mixing ratio.

Given a target ratio $T=r_1:r_2:\cdots:r_n$, where $r_i\in\mathbb{N}$ denotes the volumetric contribution of the i^{th} reagent, our method constructs a flow graph referred to as **mix-flow tree** G, where (1) each leaf node corresponds to an inlet, (2) internal nodes represent channel junctions, (3) the root node corresponds to the final outlet of the mixer, and (4) edges represent channels and the edge weights denote the assigned flow rates. The G implies a sequence of flow mixing, where each internal node has exactly two in-edges and one out-edge. The goal is to construct a layout corresponding to a G, where

all inlets can be driven by a single pressure source, and the resulting solution at the outlet accurately reflects the target ratio.

Simple one-step or sequential mixers are limited in their ability to control interfacial diffusion between reagents, which affects mixing quality. To enhance diffusion and homogeneity, we decompose each reagent's volumetric contribution into multiple sub-volumes, treating them as unique flow rates at different inlets of the μ -MM. This results in more junctions and more interleaving of reagent fronts, thereby increasing mixing efficiency. To perform this decomposition in a structured and controllable manner, we represent each r_i in a chosen base d as $r_i(\text{base } d) = r_{i,1} \ r_{i,2} \ \cdots \ r_{i,k-1} \ r_{i,k}$, allowing us to express each quantity as a sum of scaled powers of the base:

$$r_i = r_{i,1} \cdot d^{k-1} + \dots + r_{i,k-1} \cdot d^1 + r_{i,k} \cdot d^0,$$

where $r_{i,t} \in \mathbb{N}_0$ for $t \in \{1,2,...,k\}$ are the coefficients in the base d representation. For each term $r_{i,t} \cdot d^{k-t}$, we define $v_{i,t} = r_{i,t} \cdot d^{k-t}$, and treating it as the t^{th} decomposed value of r_i . For instance, if $r_i = 111, k = 3$ and d = 8, then $111 = 1 \cdot 8^2 + 5 \cdot 8^1 + 7 \cdot 8^0$, i.e., 111(base 8) = 157, where $r_{i,1} = 1, r_{i,2} = 5, \ r_{i,3} = 7$, and similarly $v_{i,1} = 1 \cdot 8^2 = 64, v_{i,2} = 5 \cdot 8^1 = 40, v_{i,3} = 7 \cdot 8^0 = 7$.

Moreover, the number of decomposed values (here k) is considered as the decomposition size. The positive decomposed values $v_{i,t}$ are used to construct the mix-flow tree, where they are considered as flow rates at different inlets of μ -MM to collectively preserve the total reagent volumetric ratio at the outlet. To have a balanced layout with proportional channel lengths and an improved mixing quality, we need to choose a suitable decomposition size. For n reagents and a decomposition size of k, the number of leaf nodes (inlets) will be in the range of $[n + k - 1, n \cdot k]$, while internal nodes (junctions) in the resulting tree (layout) lie between $[n+k-2, (n \cdot k)-1]$. Since the design complexity of the layout is proportional to the number of inlets and channel junctions, for simplicity, in this work, we consider k to be in the range of [3, 5]. In general, n ranges between [2, 10], so for the most complex layout we will have 49 channel junctions, where n = 10 and k = 5.

Once k is chosen, we need to select the base d for each reagent r_i . To get a suitable decomposition of the reagents, we first determine the valid range of base values $d \in \mathbb{N}$. Let $\bar{r} = \max(r_1, r_2, \dots, r_n)$. Then, a valid $d \in \mathbb{N}$ must satisfy:

$$d^{k-1} \leq \bar{r} \leq d^k \quad \text{ and } \quad 2 \leq d \leq \left\lfloor \bar{r}^{1/(k-1)} \right\rfloor.$$

For instance, T=41:11:111:13:4 and k=3, then d must satisfy $d^2 \leq 111 \leq d^3$ and $2 \leq d \leq 111^{\frac{1}{2}}$. From these two constraints, we can derive the list $L=\{5,6,7,8,9,10\}$ of valid bases d. Now, for an r_i , we can compute $v_{i,t}^j=r_{i,t}\cdot d_j^{k-t}$ for each $d_j\in L$ to compose a decomposition list:

$$D_{i,j} = \left[v_{i,k}^j, v_{i,k-1}^j, \dots, v_{i,1}^j \right]_{d_j},$$

Accordingly, for each r_i , we compute all the corresponding decomposition lists $D_{i,1}, D_{i,2}, \cdots, D_{i,|L|}$, from which we will

choose the "best" <u>base</u>. Specifically, we select the $\underline{d_j}$ (where j=[1,|L|]) as the "best" for which the smallest decomposed component $(v_{i,k}^j=r_{i,k}\cdot d_j^0)$ is maximized and the largest $(v_{i,1}^j=r_{i,1}\cdot d_j^{k-1})$ is minimized. Simultaneously, we also prioritize those lists $D_{i,j}$ which have the most number of zeros $(v_{i,t}^j=0)$, promoting balance and minimizing unproportional channel lengths in the layout. After selecting the "best" d_j for each r_i , we store them in a list D and construct the matrix V of size $n\times k$, consisting of decomposed values $v_{i,t}^j$:

$$V = \begin{bmatrix} v_{i,1}^j & v_{i,2}^j & \cdots & v_{i,k}^j \\ \vdots & \ddots & \ddots & \vdots \\ v_{i',1}^{j'} & v_{i',2}^{j'} & \cdots & v_{i',k}^{j'} \end{bmatrix}.$$

Finally, the proposed mix-flow tree G is generated using V, where the number of positive $v_{i,t}^j\ (>0)$ denotes the number of leaf nodes in G, and $v_{i,t}^j$ is the leaf-edge weight. We go through each column of V from left to right, pick pairs of positive values, and use them as leaf edge weights to build the G. After merging the selected pairs of edges, we get a new set of internal nodes. Considering the edge weights of these internal nodes as the sum of their in-edge weights, we recursively choose two nodes at a time and merge them till we get the root node of the mix-flow tree. For the previous example T=41:11:111:13:4 and k=3, the list D, the matrix V and the corresponding mix-flow tree are shown in Fig. 3.

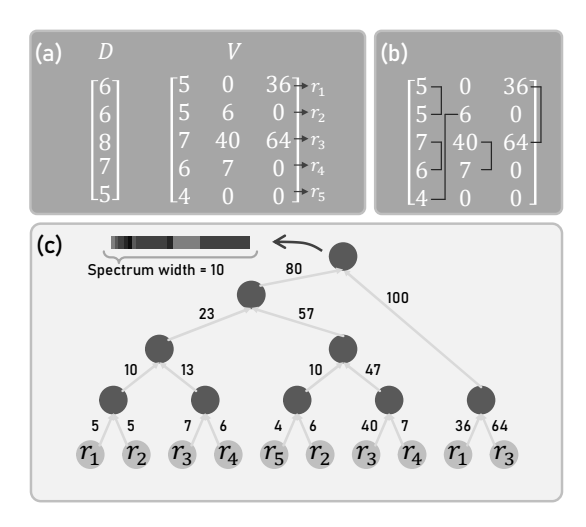


Fig. 3. Overview of ratio decomposition strategy. For T=41:11:11:13:4 (a) the chosen list of the base values D and the matrix V are determined. Then (b) pairs of values from V are selected to construct (c) the respective mix-flow tree G.

B. Layout Generation and Hydraulic Resistance Modeling

The mix-flow tree G encodes the hierarchical mixing structure and flow ratios of the target mixture. To minimize total channel lengths and enhance layout compactness, our method allows some lower-level nodes in G to be elevated to higher levels, as illustrated in Fig. 4. This transformation helps reduce path lengths and results in an **ordered tree** G' that informs the physical layout. Our layout generation algorithm translates

this abstract tree into a planar, block-based design, where the edge weight of the i^{th} edge corresponds to the flow rate Q_i . Since the flow rate is based on the hydraulic resistance, and the resistance is proportional to the length l_i of each microfluidic channel, we achieve the desired mixing ratios by carefully adjusting the lengths of channels from the inlets to the outlet. In this way, the abstract contribution values computed in the tree are faithfully realized as physical flow paths with proportional resistances.

To systematically construct the layout, we adopt a *multi-level block placement strategy*, as illustrated in Fig. 5, where each edge in G' corresponds to a physical building block. Specifically: (1) each leaf edge e_i of G' is assigned an **inlet block** α_i , (2) each internal sibling edge pair (e_j, e_{j+1}) corresponds to a **merging block** β_k .

Each inlet block is characterized by three parameters: height (\mathbb{h}), width (\mathbb{w}), and $channel\ length$ (\mathbb{I}). To simplify alignment and fabrication, the values of \mathbb{h} and \mathbb{w} are fixed for all inlet blocks. An inlet block α_i is composed of a $serpentine\ channel\ s_i$ and a short $connecting\ channel\ c_i$, where $\mathbb{I}_i = |s_i| + |c_i|$. This length determines the hydraulic resistance of the inlet channel and thus controls the flow rate for a given input pressure.

Inlet blocks are arranged horizontally following the order of the leaf nodes in G'. Each merging block receives two inputs in_{left} and in_{right} , merges the underlying outputs, and produces one output out. Its width (w) is the sum of the widths of the merged underlying blocks. To maintain uniform vertical alignment, all outlets at the same level share a common Y-coordinate (y_{out}) , ensuring uniform block height (h), which is calculated as $\mathbb{h} = y_{out} - y_{in_{right}}$, as shown in Fig. 6.

The merging block composes two straight connecting channels c_{left} and c_{right} , merging the output from the left and right underlying blocks. The length of c_{left} and c_{right} is calculated by the Euclidean distance between the corresponding input and the output of this block.

To ensure correct flow distribution across all branches, we model the fluid dynamics using the *electronic-hydraulic* analogy under laminar flow. In this analogy: (1) flow rate Q corresponds to electric current, (2) pressure drop ΔP corresponds to voltage drop, and (3) hydraulic resistance, proportional to the channel length l, corresponds to electrical resistance.

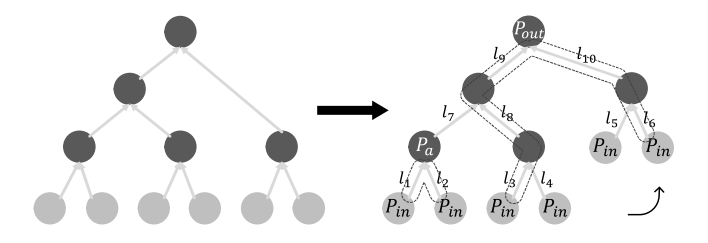


Fig. 4. Transformation of the hierarchical mix-flow tree into an ordered tree representing the layout for μ -MM. The initial tree (left) encodes the target mixing hierarchy and flow contributions. To reduce the total channel length in the physical realization, some nodes are elevated to higher levels, resulting in the ordered tree (right). It serves as an intermediate, layout-aware representation that informs the final planar physical design.

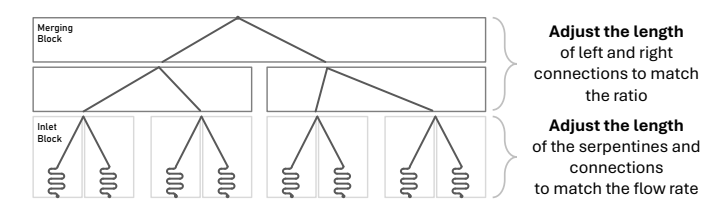


Fig. 5. Schematic of block placement strategy for the ordered tree layout.

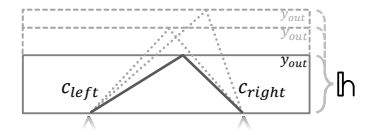


Fig. 6. The height of a merging block is determined by the output position where the left and right channels converge.

In order to maintain the correct flow rate ratio at each junction, we will use the previously mentioned analogy to consider the length of the connecting channels. By applying the analogy, Hagen-Poiseuille's law can be simplified as: $\Delta P = QR_H$, where Q and R_H define the volumetric flow rate and the hydraulic resistance, respectively.

As our proposed μ -MM is single-pressure-driven, the incoming pressure at each inlet is the same. Hence, two paths starting from any two inlets and having a common junction in G' are analogous to a parallel connection in an electric circuit. Which implies that the pressure drops along both paths are equal: $\Delta P_{path1} = \Delta P_{path2}$. For instance, in Fig. 4, the pressure drop at the a^{th} junction is $P_{in}-P_a$, while the channel lengths l_i must satisfy $l_1 \cdot Q_1 = l_2 \cdot Q_2$. Similarly, for two paths across multiple levels, such as $(l_3, l_8, l_9) : (l_6, l_{10})$, merging at the outlet node, the pressure drop is $P_{in}-P_{out}$, where we have $l_3 \cdot Q_3 + l_8 \cdot Q_8 + l_9 \cdot Q_9 = l_6 \cdot Q_6 + l_{10} \cdot Q_{10}$.

All layout constraints are defined in a *constraint optimization programming (COP) formulation* that includes: (1) correct flow distribution through recursive resistance matching, (2) geometric alignment across block levels, (3) layout constraints such as channel length, number of turnings of the serpentine, and serpentine properties, and (4) block height and the output coordinates, automatically computed based on feasible path lengths. Here, the objective is to minimize the total channel length, which implies the optimization of the layout area. The optimization result ensures that the generated layout meets all the constraints and is physically manufacturable and hydraulically functional.

After constructing the full 2D layout, each channel and junction is annotated with its flow rate and geometric dimensions. This annotated layout is then converted into a 3D model using geometric meshing and faceting. The finalized model can be exported in the standard .STL format for direct fabrication using commercial 3D printing technologies.

IV. EXPERIMENTAL RESULTS

To validate our proposed μ -MM, we implemented the proposed synthesis method in Java and evaluated its performance

on an Apple Silicon M1 MacBook Pro with 8 cores (4 performance and 4 efficiency) and 16 GB of memory. The constrained optimization subproblems required for computing channel lengths and ensuring hydraulic resistance alignment were formulated as a quadratic mathematical model and solved using the Gurobi Optimizer [23]. We conducted a series of experiments and simulations involving both real-world and synthetic reagent mixing scenarios.

A. Test Cases

We selected four reagent mixing scenarios from common microfluidic workflows: (1) sample preparation for ChIP assay [24], (2) sample preparation for protein electrophoresis [25], (3) Taq DNA PCR test [26], and (4) ChIP lysis buffer preparation [27]. For each case, the desired reagent mixing ratios were extracted from established laboratory protocols. Our synthesis method automatically generated customized microfluidic layouts by decomposing the target ratios into finer components to match flow volumes under a single pressure source. The resulting designs include the necessary branching structures, channel lengths, and inlets to enforce the correct volumetric contributions via controlled hydraulic resistance. The generated designs were fabricated using a hobby-grade 3D-printer—Elegoo Mars 5. We validated each design through finite element simulation using COMSOL Multiphysics [28], modeling the laminar mixing based on solute concentration. Given the limitations within COMSOL Multiphysics regarding the visual differentiation of reagents by color, disparate reagents were modeled by assigning them unique inlet concentrations. This approach enabled us to visually distinguish reagents through color variation. In each case, for contrast and clarity, solute concentrations were set as follows: R1 = 0.4mol/L (blue-green), R2 = 0.9 mol/L (red), R3 = 0.65 mol/L(yellow), R4 = 0.2 mol/L (blue), R5 = 0.75 mol/L (orange), R6= 0.55 mol/L (yellow-green), and R7 = 0.35 mol/L (cyan). The simulation results were then compared to the theoretical target concentrations for each case. Across all four experimental cases, the simulated outlet concentrations deviated by less than 0.01 mol/L from the expected target values, confirming the effectiveness and precision of our layout choice and synthesis method. Figure 7 summarizes the full pipeline for each case: from input ratio and synthesized layout to 3D CAD model, printed chip, and final simulation results, while Table I (1)– (4) summarize the corresponding performance metrics.

In addition to above mentioned four real-world scenarios, we also evaluated our method on four synthetic mixing ratios. While figures for these synthetic cases are not included in the paper, their performance metrics are listed in Table I (5)–(8).

The table reports performance metrics of the testcases as follows: (i) the *spectrum width* (i.e., number of unique laminar sub-flows generated at the outlet), which directly implies the degree of homogeneity of the mixture at the output; (ii) the *chip footprint*, which indicates the size of the synthesized layout; (iii) the *total channel length*, which is proportional to the total hydraulic resistance (R_H) of the chip; (iv) the

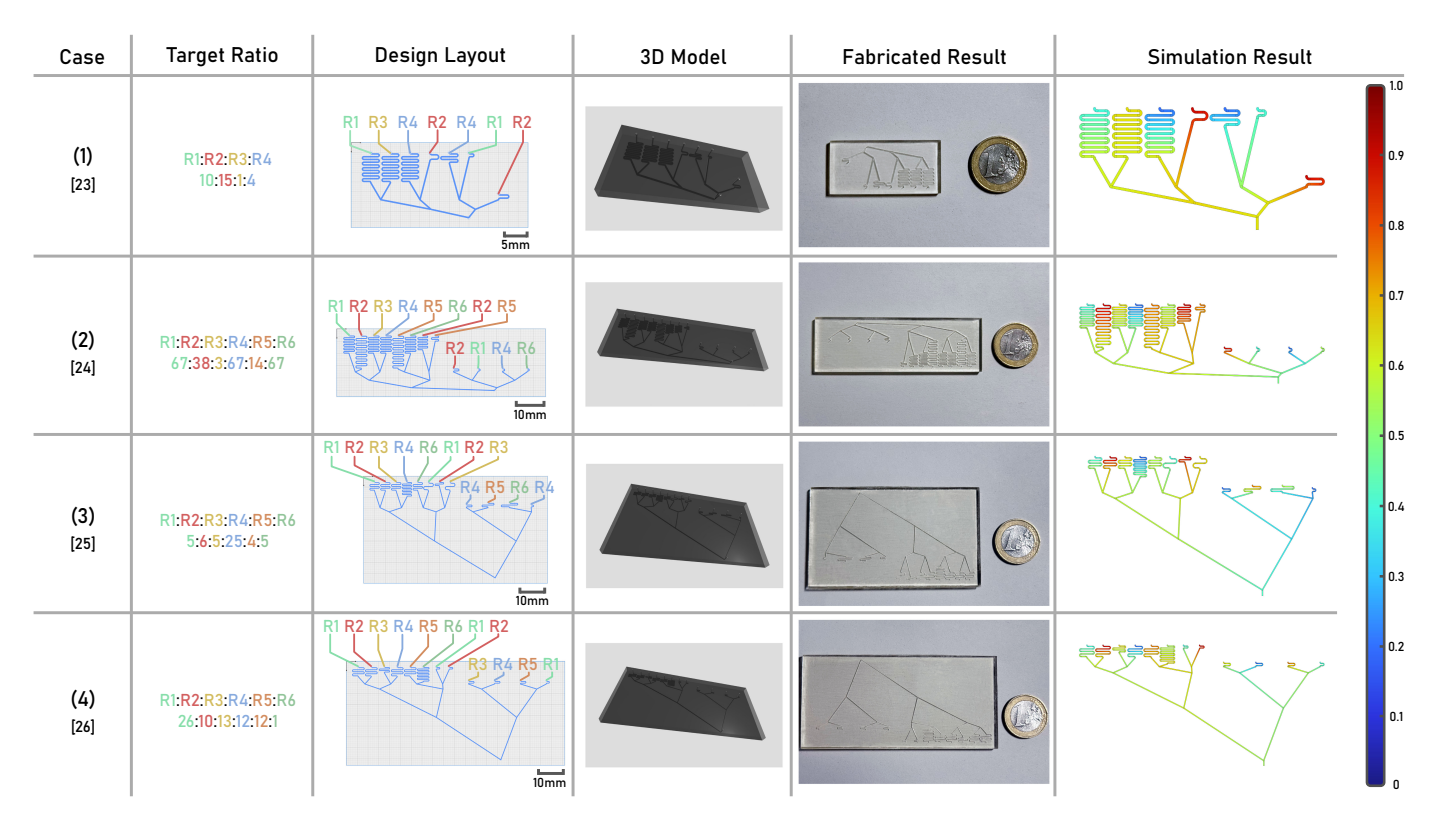


Fig. 7. Real-world microfluidic mixing scenarios synthesized using our proposed μ -MM. Each row corresponds to a unique test case. The first column indicates the case number. The second column presents the target mixing ratio of reagents (R1, R2, ...), color-coded for clarity, and corresponds to the simulation result. The third column shows the automatically synthesized design layouts. The fourth column displays the corresponding print-ready 3D models. The fifth column presents photographs of the 3D-printed and fabricated microfluidic chips. The sixth column shows simulation results of solute concentration distribution across the chip layout. Simulations are based on laminar flow and solute transport; the color bar represents solute concentration in mol/L.

TABLE I SUMMARY OF CASE STUDIES

		Proposed Method					Baseline Method			
Case	Target Ratio	Spectrum Width	Chip Footprint	Total Channel Length	Runtime	Deviation	Spectrum Width	Chip Footprint	Total Channel Length	Runtime
			$(in \ \mu m^2)$	(in μm)	(in ms)	(in mol/L)		$(in \mu m^2)$	(in μm)	(in ms)
(1)	10:15:1:4	7	24031×45000	265330	144	+0.009	30	60247×165000	1930851	194
(2)	67:38:3:67:14:67	12	27559×85000	583689	125	+0.005	88	_	_	_
(3)	5:6:5:25:4:5	12	49582×85000	433945	145	+0.002	16	19608×85000	549716	201
(4)	26:10:13:12:12:1	12	48073×101000	427578	139	+0.002	74	_	_	_
(5)	3:1:5:2:1:1:2	9	13126×55000	192293	142	-0.016	15	90194×85000	540345	236
(6)	3:1:2	4	11724×25000	83822	108	+0.006	6	27547×45000	224863	136
(7)	2:1:4:2:1:1:1	8	31265×45000	374986	113	-0.011	13	36732×75000	741057	158
(8)	23:15:11	7	27536×45000	243418	120	-0.012	6	21677×45000	263917	148

*The dash (—) indicates that the synthesis result will not be available after 5 minutes of runtime

synthesis *runtime*; (v) and the *deviation* between the target ratio and the simulated result.

B. Baseline Comparison

Since the proposed μ -MM is the first synthesis method targeting ratio-specific multi-reagent mixing under a single-pressure input, we introduce a custom baseline for comparative purposes. The baseline method decomposes all reagent ratios to units of the smallest ratio value (e.g, $\underline{10}$:4 is decomposed into $\underline{4:4:2:4}$) and shuffles them to maximize the spectrum width. For the layout generation, we use the proposed block placement strategy.

While this baseline generally achieves a broader mixing spectrum—potentially leading to better homogeneity—the resulting microfluidic layouts typically involve longer channels and, in most cases, are significantly larger, with more junctions

and inlet branches. This increased complexity implies: (1) higher material consumption, (2) longer fabrication time, (3) increased potential for fabrication errors, (4) greater post-print and post-use cleaning difficulty, and (5) higher flow resistance, increasing pressure and energy demand. Table I also compares our method and the baseline across the presented eight cases, demonstrating the trade-off between mixing granularity and physical layout complexity. In most cases, our method yields significantly more compact and manufacturable designs, with reduced chip footprint and total channel length. While the baseline exhibits a wider spectrum—indicating improved mixing homogeneity—this comes at the cost of a more complex channel network and higher total hydraulic resistance R_H . These results highlight the effectiveness of the proposed ratio decomposition heuristic in balancing homogeneity with layout efficiency.

V. CONCLUSION

Mixing multiple reagents in precise ratios is a fundamental requirement in microfluidic systems, with applications ranging from biochemical assays to molecular diagnostics. However, designing compact, 3D printing manufacturable chips that achieve accurate mixing ratios, especially under a single pressure input, remains a challenge. In this work, we proposed a novel design synthesis method for ratio-specific mixing in 3D-printed microfluidic chips. Our approach decomposes complex reagent ratios into smaller sub-ratios and automatically generates channel layouts with appropriate hydraulic resistance to ensure accurate volumetric flow under uniform pressure, with minimal hardware complexity. We validated the method through a combination of real-world case studies, synthetic scenarios, 3D printing fabrication, and COMSOLbased simulations. Across all eight test cases, the synthesized designs demonstrated excellent mixing ratio precision while maintaining compact footprints and manageable fabrication complexity. This synthesis approach offers a scalable, automated pathway for designing single-pressure, multi-reagent mixers, potentially democratizing the deployment of custom microfluidic devices in research and diagnostics.

ACKNOWLEDGEMENT

This work is supported by the Deutsche Forschungsgemeinschaft (DFG, German Research Foundation) – Project Number 515003344.

REFERENCES

- [1] K. F. Lei, "Microfluidic systems for diagnostic applications: A review," *Journal of laboratory automation*, vol. 17, no. 5, pp. 330–347, 2012.
- [2] K. S. Elvira, X. C. i Solvas, R. C. Wootton, and A. J. Demello, "The past, present and potential for microfluidic reactor technology in chemical synthesis," *Nature chemistry*, vol. 5, no. 11, pp. 905–915, 2013.
- [3] T. J. Johnson, D. Ross, and L. E. Locascio, "Rapid microfluidic mixing," Analytical chemistry, vol. 74, no. 1, pp. 45–51, 2002.
- [4] Y. Zhang, M. Li, T.-M. Tseng, and U. Schlichtmann, "Open-source interactive design platform for 3d-printed microfluidic devices," *Com*munications Engineering, vol. 3, no. 1, p. 71, 2024.
- [5] C.-Y. Lee, W.-T. Wang, C.-C. Liu, and L.-M. Fu, "Passive mixers in microfluidic systems: A review," *Chemical Engineering Journal*, vol. 288, pp. 146–160, 2016.
- [6] Z. Li, B. Zhang, D. Dang, X. Yang, W. Yang, and W. Liang, "A review of microfluidic-based mixing methods," *Sensors and Actuators A: Physical*, vol. 344, p. 113757, 2022.
- [7] J. Wang, P. Brisk, and W. H. Grover, "Random design of microfluidics," Lab on a Chip, vol. 16, no. 21, pp. 4212–4219, 2016.
- [8] A. Agrawal and S. Roy, "Random microfluidic chip design with diagonal channels using k-means clustering for fluid dilutions," in 2024 IEEE Computer Society Annual Symposium on VLSI (ISVLSI). IEEE, 2024, pp. 100–105.
- [9] J. Wang, N. Zhang, J. Chen, G. Su, H. Yao, T.-Y. Ho, and L. Sun, "Predicting the fluid behavior of random microfluidic mixers using convolutional neural networks," *Lab on a Chip*, vol. 21, no. 2, pp. 296– 309, 2021.
- [10] U. Bilitewski, M. Genrich, S. Kadow, and G. Mersal, "Biochemical analysis with microfluidic systems," *Analytical and bioanalytical chemistry*, vol. 377, no. 3, pp. 556–569, 2003.
- [11] P. S. Dittrich and A. Manz, "Lab-on-a-chip: microfluidics in drug discovery," *Nature reviews Drug discovery*, vol. 5, no. 3, pp. 210–218, 2006.
- [12] X. Wang, Z. Liu, and Y. Pang, "Concentration gradient generation methods based on microfluidic systems," *RSC advances*, vol. 7, no. 48, pp. 29966–29984, 2017.

- [13] S. Marre and K. F. Jensen, "Synthesis of micro and nanostructures in microfluidic systems," *Chemical Society Reviews*, vol. 39, no. 3, pp. 1183–1202, 2010.
- [14] Y. Zhang, D. Rašeta, T.-M. Tseng, and U. Schlichtmann, "3m-desyn: Design synthesis for multi-layer 3d-printed microfluidics with timing and volumetric control," in *Proceedings of the 30th Asia and South Pacific Design Automation Conference*, 2025, pp. 1357–1363.
- [15] J. Nam and C. S. Lim, "Micromixing using swirling induced by three-dimensional dual surface acoustic waves (3d-dsaw)," Sensors and Actuators B: Chemical, vol. 255, pp. 3434–3440, 2018.
- [16] P. Modarres and M. Tabrizian, "Phase-controlled field-effect micromixing using ac electroosmosis," *Microsystems & Nanoengineering*, vol. 6, no. 1, p. 60, 2020.
- [17] Y. Wang, J. Zhe, B. T. Chung, and P. Dutta, "A rapid magnetic particle driven micromixer," *Microfluidics and Nanofluidics*, vol. 4, pp. 375–389, 2008
- [18] S. Bhattacharjee, S. Poddar, S. Roy, J.-D. Huang, and B. B. Bhattacharya, "Dilution and mixing algorithms for flow-based microfluidic biochips," *IEEE Transactions on Computer-Aided Design of Integrated Circuits and Systems*, vol. 36, no. 4, pp. 614–627, 2016.
- [19] D. Kundu, S. Roy, S. Bhattacharjee, S. Saha, K. Chakrabarty, P. P. Chakrabarti, and B. B. Bhattacharya, "Mixing models as integer factorization: A key to sample preparation with microfluidic biochips," *IEEE Transactions on Computer-Aided Design of Integrated Circuits and Systems*, vol. 41, no. 3, pp. 558–570, 2021.
- [20] K. Ward and Z. H. Fan, "Mixing in microfluidic devices and enhancement methods," *Journal of Micromechanics and Microengineering*, vol. 25, no. 9, p. 094001, 2015.
- [21] Y. Chen, T. Sun, Z. Liu, Y. Zhang, and J. Wang, "Towards design automation of microfluidic mixers: Leveraging reinforcement learning and artificial neural networks," *Micromachines*, vol. 15, no. 7, p. 901, 2024.
- [22] N. Zhang, Z. Liu, and J. Wang, "Machine-learning-enabled design and manipulation of a microfluidic concentration gradient generator," *Micromachines*, vol. 13, no. 11, p. 1810, 2022.
- [23] Gurobi Optimization, LLC, "Gurobi Optimizer Reference Manual," 2025. [Online]. Available: https://www.gurobi.com
- [24] Illumina, Inc., "Preparing Samples for ChIP Sequencing of DNA," 2007. [Online]. Available: https://genome.med.harvard.edu/documents/illumina/11257047_ChIP_Sample_Prep.pdf
- [25] OpenWetWare, "Sean Lauber: SDS-PAGE Protein Electrophoresis," 2013. [Online]. Available: https://openwetware.org/wiki/Sean_Lauber:SDS_PAGE_Protein_Electrophoresis
- [26] Ampliqon A/S, "Taq DNA Polymerase 2x Master Mix RED," 2025. [Online]. Available: https://ampliqon.com/api/ampliqon/downloaddatasheet?variant=A180303
- 27] Abcam Inc., "A Beginners Guide to ChIP," 2011. [Online]. Available: https://docs.abcam.com/pdf/chromatin/A-beginners-guide-to-ChIP.pdf
- [28] COMSOL AB, Stockholm, Sweden, "COMSOL Multiphysics®," 2025. [Online]. Available: https://www.comsol.com/